Machine Studies of TLS

The major machine studies undertaken in the years of 2001/2002 are summarized in the following paragraphs.

Dynamic Tuning of Insertion Device

Due to the vertical tune drift during gap change of insertion device U9, coupling resonance and hence the sudden change of beam size were frequently observed. We have implemented a tune correction scheme in order to reduce this effect. In addition to the tune correction during U9 gap change, the dynamic orbit corrections using follow-gap end correctors, in combination with the digital global orbit feedback during gap changes of U5, EPU, and U9, demonstrate good beam orbit stability during routine operation.

Nonlinear Beam Dynamics Experiments

Using phase space monitors consisting of turn-by-turn beam position monitors (BPM's), nonlinear beam dynamics studies were conducted to characterize the lattice parameters, such as detuning factor and strengths of the nonlinear resonances. The resonance strengths around 3rd-order, 4th-order, as well as 5th-order nonlinear parametric resonance points were measured. It is found that the resonance strengths can be reproduced with a set of magnetic field errors. This set of field errors is consistent with the measured magnetic field errors. Fig. 1 shows the measured detuning behavior and Fig. 2 depicts the Poincare phase-space map of 3rd-order resonance. Fig. 3 is the corresponding action-angle plot.

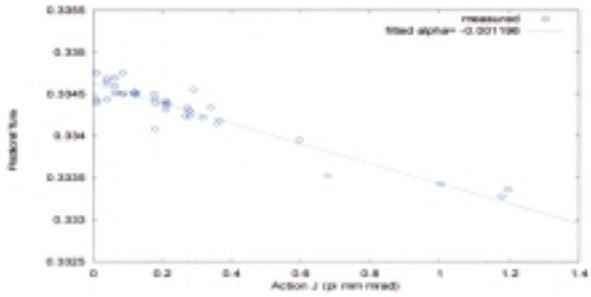

Fig. 1: De-tuning parameter around third-order resonance line. α = -0.0012 $\pm$0.0001 (π mm mrad)$^{-1}$

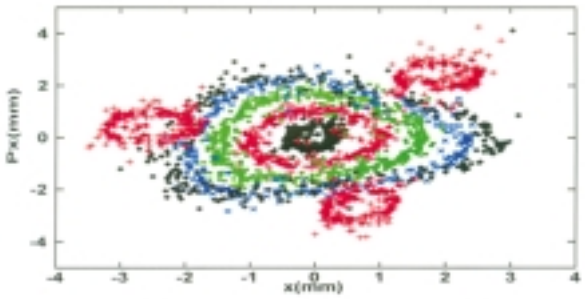

Fig. 2: Poincare map near third-order resonance.

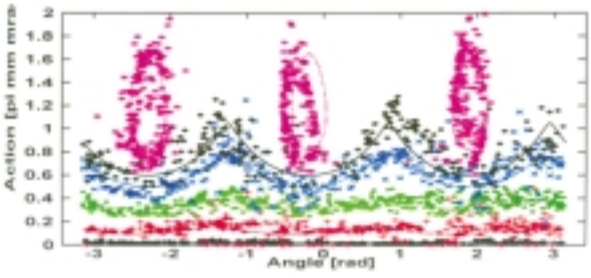

Fig. 3: Action-angle near third-order resonance line.

Longitudinal Beam Dynamics of RF Modulation and Its Applications

The effects of RF cavity voltage modulation on longitudinal beam dynamics were studied at the Taiwan Light Source (TLS). Theoretical description of RF voltage modulation that includes the effect of non-zero synchronous phase has been developed. The formation of beamlets in the bucket helps to damp the coherent coupled bunch oscillation driven by parasitic modes of the RF cavity. This beam manipulation technique has been successfully employed to provide stable beam operation at the TLS. For detailed description please refer to the section "Accelerator and Insertion Device R&D".

Coupling Correction

After installing eight independent skew quadrupole magnets in the storage ring, we were able to correct betatron coupling as well as vertical dispersion to an acceptable value, depending on the balance of the beam current lifetime and beam brightness in the routine operation. Fig. 4 shows the typical beam size images before and after the coupling corrections during routine operation.

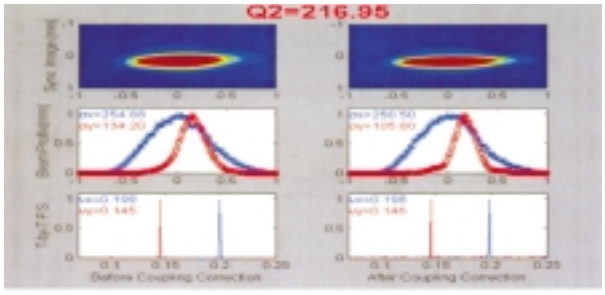

Fig. 4: Typical beam size images before and after the coupling correction during routine operation.

TLS-II Lattice Design

To provide high intensity synchrotron light at higher photon energy than that can be generated by the current 1.5 GeV ring, a feasibility study of a 3 ~ 3.5 GeV intermediate energy ring, designated TLS-II, has been initiated. The maximum allowed ring circumference is 240 m due to site limitation. Several options of the ring lattices have been studied and optimization of the beam dynamics behavior is in progress.

Status of the SRF Project

To prepare for the installation and operation of the SRF system in 2003, not only the SRF module, but also the transmitter, the low level RF control system, and high power RF components like circulator, RF load etc., have to be ready in the year 2002. To meet the SRF project schedule, the major work load of the RF group this year includes setting up the SRF subsystems and testing the performance of the high power components, in addition to the routine maintenance of RF systems. Current status of the subsystems and high power components is described in the following paragraphs.

A new transmitter is assembled with a spare klystron based on the existing design but with 1/3 more output power. In order to handle the higher output power, we redesign a RF coupler. In April 2002 this transmitter was successfully tested with RF output power up to 80 kW. For reliability test, this transmitter has been continuously operated with 60 kW output power for one week without trip.

A spare low level RF system will be used to control the RF phase, cavity gap voltage, and the resonant frequency of the SRF cavity. The subsystem has been tested with the conventional cavity, and test result shows that this RF control system functions well. For matching the new design on the tuner drive for the SRF module, we have modified the tuner drive circuit module and test of the modified module is underway.

All the RF waveguide components for assembling the RF transmission line have been acquired. The two high power circulators had been tested with RF power up to 60 kW in April 2002. In this test, a high power RF load was used to absorb the RF power. The sliding short position was adjusted in a wide range to measure the isolation performance and the figure is always better than 24 dB at any reflection RF phase.

After the test of subsystems and high power RF components of the SRF system is completed, the new transmitter and the low level RF system will be moved from the booster area where the test is

done to the final position in core area in May or June 2002. Assembling of the transmission line components and integrating the subsystems for the SRF module operation will follow. We expect that all the integrated subsystems will be tested before the arrival of the SRF module in 2003.

Design and Fabrication of Thyratron Pulser

The major component of the booster pulse power supplies is basically a thyratron tube. In order to trigger the thyratron tube a pulse source with very high stability is needed. The pulse driver currently used in booster ring is of the commercial, general-purpose type. The pulse reflection and ringing frequently cause damage on power MOS in the driver circuitry. To address this problem, a new circuit configuration of pulse driver was designed in-house. The circuitry of SRRC-1000 thyratron driver is composed of IGBT, optical coupler, and isolation power source, as shown in Fig. 5. After a series of tests on stability and reliability, the new driver easily achieved a timing jitter of ± 0.2 ns in a period of 4 hours and then was installed in booster ring for driving the extraction kicker. In Fig. 6 the output of the SRRC-1000 pulser is compared with that of a DEI-1000 commercial pulse driver. Fig. 7 shows the inside of SRRC-1000 pulser system now in daily service in the booster ring.

MATLAB - Control System Interface

To provide a better environment for control

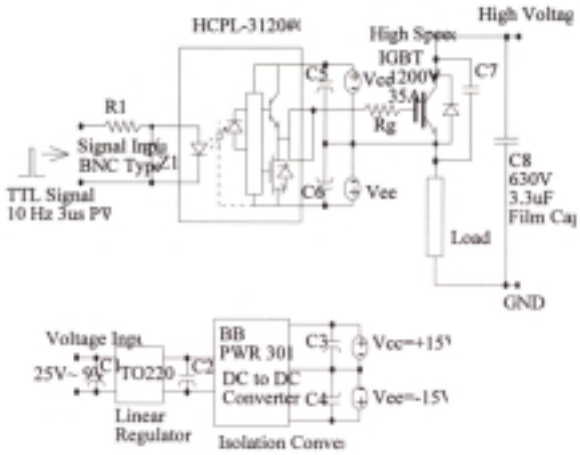

Fig. 5: Circuit configuration of new thyratron pulse driver.

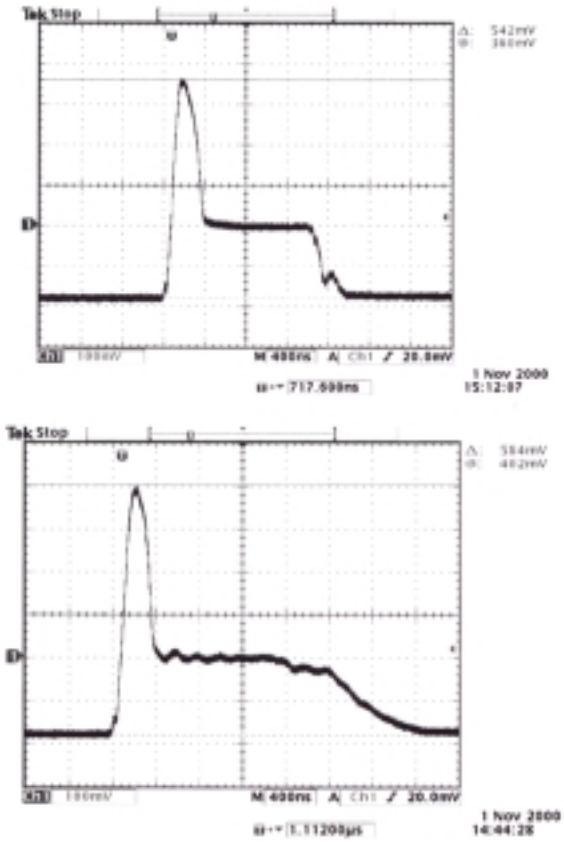

Fig. 6: (a) High voltage pulse signal measured at grid 2 of CX1159 with DEI-100 pulser. (b) High voltage pulse signal measured at grid 2 of CX1159 with SRRC-1000. (Scale : 1V=1000V)

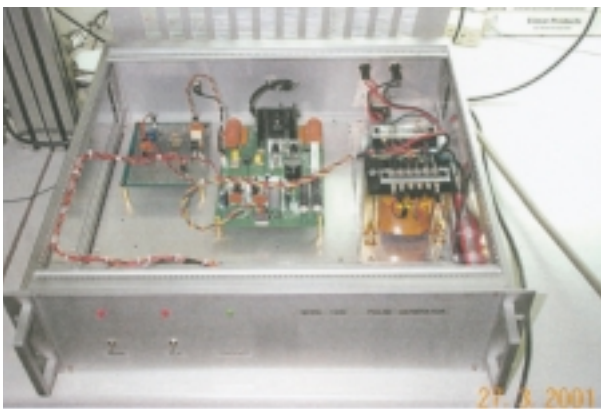

Fig. 7: Inside the SRRC-1000 thyratron pulse driver.

algorithm prototyping and to support various machine study requirements, MATLAB control system interface was implemented. Using MATLAB environment to develop, test, and run the control algorithms has proven to be a fast and efficient way to accommodate the requirements of the storage ring of SRRC. The implementation includes MATLAB scripts for database access,

scripts for IEEE-488 instruments access, and various accelerator related scripts.

A typical example of MATLAB application is the gap voltage modulation technique used in routine operation to eliminate the longitudinal instability in the storage ring of SRRC. The mechanism of instability elimination is investigated by systematic observation of the evolution of synchrotron oscillation sideband as function of modulation amplitude and frequency. The schematic diagram of the experimental setup is shown in Fig. 8. MATLAB scripts were used to perform the study. Fig. 9 shows typical synchrotron sideband evolution as a function of modulation frequency of one sideband. It clearly demonstrates that the instability sideband is suppressed when modulation frequency is approximately two times the synchrotron oscillation frequency.

Turn-by-Turn BPM System

Turn-by-turn BPM system was implemented, and three sets of log-ratio BPM processors were installed at the storage ring as well as the booster synchrotron. The turn-by-turn beam position is digitized by the multi-channel digitizer, which is clocked by the revolution clock of the storage ring and the booster synchrotron. Turn-by-turn BPM system of the storage ring was used for various studies including injection tune monitoring, nonlinear resonance, and coupling study. The turn-by-turn BPM system for the booster synchrotron are used to observe tune evolution during energy ramping and coupling resonance study. Fig. 10 shows the tune variation of the booster during energy ramping.

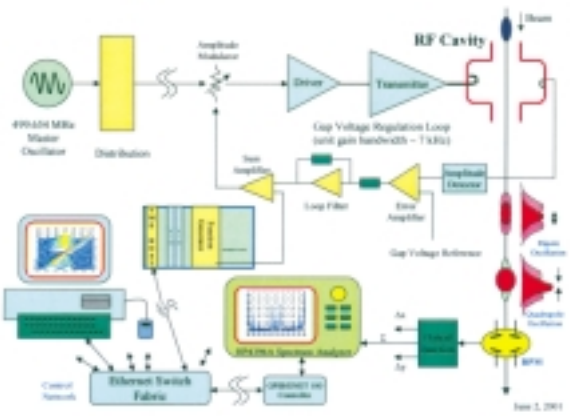

Fig. 8: Setup of the gap voltage modulation experiment.

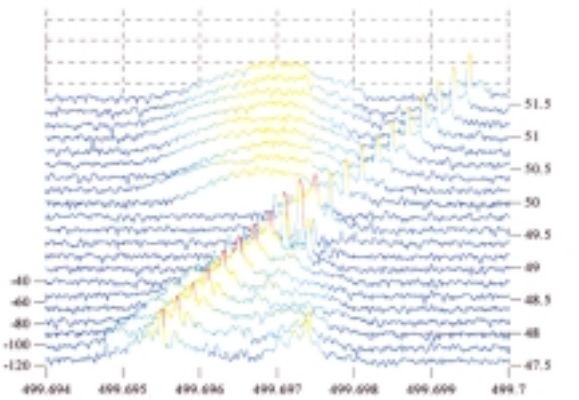

Fig. 9: Synchrotron sideband evolution as a function of modulation frequency.

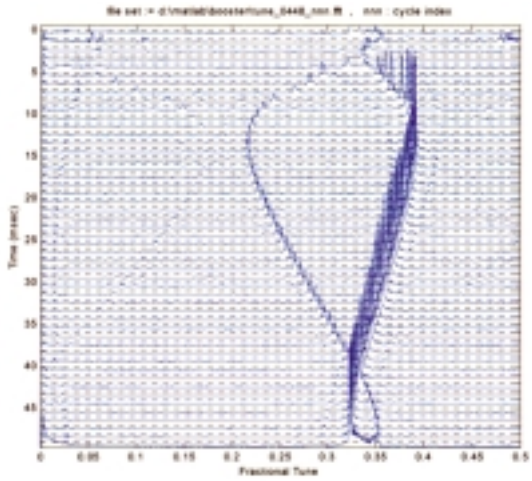

Fig. 10: Tune variation during energy ramping.

Utility Upgrade

The Utility Center accomplished the following major projects in 2001: upgrade of electric power system, temperature control of storage ring tunnel, and improvement of de-ionized cooling water system.

The electric power system now incorporates a SCADA (Supervisory Control And Data Acquisition) system which remotely monitors and controls the electric power supplied to the ring. Data collected by SCADA in Fig. 11 reveal that the ±6% μm fluctuation in horizontal beam size is correlated with the ±3% variation in line voltage, which is the nominal value specified by

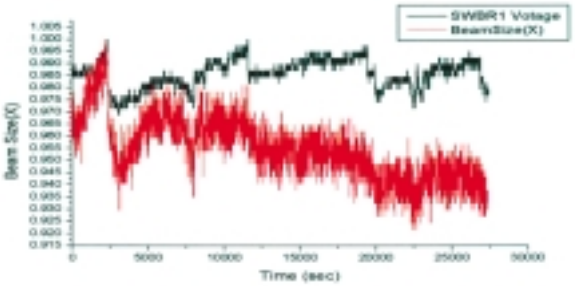

Fig. 11: Normalized variation of horizontal beam size vs. voltage

the Taiwan Power Company. Follow-up research and improvement have been done to address the problem. Also a new grounding system with low resistance was contracted and scheduled to be completed in 2002.

The control program for air conditioning system was implemented with dead band control logarithm to reduce over- and under-shooting temperature in the storage ring tunnel, resulting in ±0.1℃~0.2℃ accuracy in 72 hours of operation. The airflow in the EPU(Elliptical Polarization Undulator) area was simulated and optimized to suppress the spatial temperature gradient. Fig. 12 (b) shows that the sensor readings are within 0.2℃, as compared with data before the improvements in Fig. 12 (a).

Temperature of the de-ionized water was improved from ± 1℃ to ± 0.15℃ and the resistivity was maintained above 1MΩ/cm at pH of 7±0.1, as shown in Fig. 13. Water quality was also improved by upgrading local filters, reverse osmosis, conductivity meters, pH monitors, accumulated flow meters, and various resins. The dissolution of oxygen, an essential factor that affects water quality, was reduced from 5000 ppb to 6 ppb by new deoxygenating equipment.

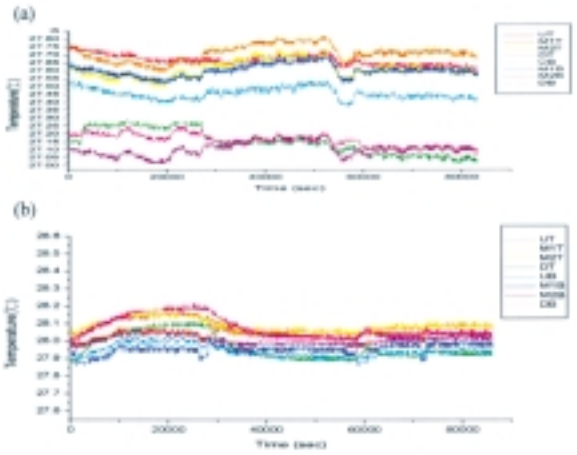

Fig. 12: Temperature variation of the EPU area. (a) before improvement; (b) after improvement.

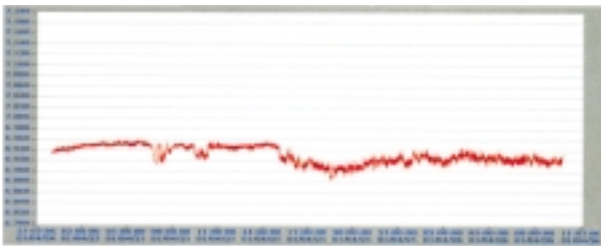

Fig. 13: pH value of deionized water over one-day period.

For further details:

K. T. Hsu (Head of Light Source Division) and J. R. Chen (Head of Instrumentation Development Division)

Synchrotron Radiation Research Center, Hsinchu, Taiwan